

Reinforcement Learning based Visual Navigation with Information-Theoretic Regularization

Qiaoyun Wu^{1,2}, Kai Xu^{3*}, Jun Wang^{1**}, Mingliang Xu⁴, and Dinesh Manocha²

¹ Nanjing University of Aeronautics and Astronautics

² The University of Maryland

³ National University of Defense Technology

⁴ Zhengzhou University

Abstract. To enhance the cross-target and cross-scene generalization of target-driven visual navigation based on deep reinforcement learning (RL), we introduce an information-theoretic regularization term into the RL objective. The regularization maximizes the mutual information between the action and the current and next visual observations of the agent. This way, the agent understands the causality between navigation actions and the changes in its observations, thus making more informative decisions. By maximizing the variational lower bound of the mutual information, we learn a generative model of the action-observation dynamics. Based on the model, the agent generates (imagines) the next observation and predicts the next action via comparing the current and the imagined next observations. Cross-target and cross-scene evaluations on the AI2-THOR framework [44] and the Active Vision Dataset (AVD) [1] show that our method attains at least 7% improvement of average success rate over some state of the art methods on the two datasets.

Keywords: Target-driven visual navigation, deep reinforcement learning, information-theoretic regularization

1 Introduction

Visual navigation is one of the basic components of an autonomous agent performing a large variety of tasks in complex environments. It can be characterized as the ability of an agent to understand its surroundings and navigate efficiently and safely to a designated target solely based on the input from on-board visual sensors [44,39,36]. This process encompasses two key components. First, the agent should be able to analyze and infer the most relevant parts from the current observation and the target, to guide the current decision. Second, the agent should understand the correlation and causality between navigation actions and the changes in the observation of its surroundings.

Recently, there is an increased interest in mapless visual navigation approaches, in which the agent neither relies on the prior knowledge of the environment, nor performing online mapping. Instead, it predicts navigation actions

* Corresponding author: Kai Xu (kevin.kai.xu@gmail.com)

** Corresponding author: Jun Wang (wjun@nuaa.edu.cn)

directly from observational pixels thanks to end-to-end deep learning, e.g., Imitation Learning [28,31,34] and Deep Reinforcement Learning [14,20,39]. Despite significant progress in visual navigation [10,33,38,43], the generalization to novel targets and unseen scenes is still a fundamental challenge. The latest work [36] proposes a self-adaptive visual navigation (SAVN) which shows strong result on novel scene adaption on AI2-THOR [44]. It does not, however, support the adaptation to novel targets. Our goal is a visual navigation, driven by targets represented by an image, with both cross-scene and cross-target generalization.

In achieving that, we propose to enhance a Deep Reinforcement Learning approach (e.g. A3C [22]) with an information-theoretic regularization. In particular, we introduce a regularization term into the standard RL objective, to guide the agent in a more informative search for its navigation actions. In particular, the regularization maximizes the mutual information between the action and the current and next visual observations of the agent. This way, the agent understands the causality between navigation actions and the changes in its observations, thus making more informative decisions.

The maximization is, however, intractable due to the unknown next visual observation at each time step. We instead maximize the variational lower bound of the mutual information. This leads to a variational auto-encoder (VAE) which generates (imagines) the next observation based on the current observation and the target view. Furthermore, we regularize the latent space of the VAE through the action-observation dynamics. The agent then predicts the next action based on the current and the *imagined* next observations. Consequently, the agent essentially builds a connection between the current observation and the target to infer the most relevant part for navigation, and make decisions based on the causality between navigation actions and observational changes.

There are several works on introducing information-theoretic regularization to RL [18,40]. Most of them strive to maximize the entropy of the policy to encourage exploration or to make the policy more stochastic for better robustness. A more related work is [23] which devises a similar mutual information maximization as an internal reward for learning intrinsically motivated agent. Different from their work, we use mutual information maximization as a regularization of the objective and learn a generative model of the action-observation dynamics. To our knowledge, our method is the first to use information-theoretic regularization to guide the learning of generalizable navigation. We conduct evaluation on datasets of both synthetic and real-world scenes, including AI2-THOR and AVD. We show that our model outperforms the state of the art [44] significant (e.g., at least 7% higher success rate for cross-scene evaluation on AVD, and 10% higher success rate for both cross-target and cross-scene evaluation on AI2-THOR). *Our code has been submitted and will be made publicly available.*

2 Related Works

Autonomous navigation in an unknown environment is one of the core problems in mobile robotics, which has been extensively studied. In this section, we provide a brief overview of some relevant works below.

Reinforcement learning. Recently, a growing number of methods have been reported for RL-based navigation [44,20,5,42,15]. For example, Jaderberg et al. [14] take advantage of auxiliary control or reward prediction tasks to assist reinforcement learning in synthetic 3D maze environments. Direct prediction of future measurements during learning also appears effective for sensorimotor control in simple immersive environments [7]. Gupta et al. [11] present an end-to-end architecture to jointly train mapping and planning for navigation in novel scenes with the perfect odometry available assumption. Savinov et al. [32] propose the use of topological graphs for the task of navigation and require several minutes of footage before navigating in an unseen scene. Kahn et al. [15] explore the intersection between model free algorithms and model-based algorithms in the context of learning navigation policies. Wei et al. [39] integrate semantic and functional priors to improve navigation performance and can generalize to unseen scenes and objects. In contrast, we incorporate imitation learning within an RL framework to further improve both the cross-target and the cross-scene generalization capability of a navigation agent.

Combined approaches. Methods combining the advantages of Imitation learning (IL) and RL have become popular [17,35,30,8,45]. These works provide suitable expert demonstrations to mitigate the low RL sample efficiency problem. Ho et al. [13] exploit a generative adversarial model to fit distributions of states and actions defining expert behavior. They learn a policy from supplied data and hence avoid the costly expense of RL. [9,16,25] share the same idea of learning from multiple teachers. Li et al. [16] discard bad maneuvers by using a reward based online evaluation of the teachers during training. Muller et al. [25] use a DNN to fuse multiple controllers and learn an optimized controller. Target-driven navigation in static environments is different from the problems above due to the easy acquisition of the optimal expert (the shortest path). Hence, there is no need to consider the bad demonstrations. On the one hand, we learn to maximize an expected long-term return provided by environments. On the other hand, we add an intermediate process to the navigation policy (the generation of the future observation) and predict an action based on the difference between the current and the future observations. This makes a more effective and generalizable target-driven navigation model.

Information-gain based approaches. Information-gain based strategies have been applied to a variety of robotics problems involving planning and control. It has been used to study optimal sensor placement and motion coordination for a target-tracking task [19], derive an information-theoretic metric as a new visual feature for visual servoing [6], optimize an information-theoretic objective to improve the informativeness of both local motion primitives and global plans for mapping [4], facilitate RL to compute good trajectories for scene exploration [2]. However, to the best of our knowledge, information-gain based strategies have

not been applied to the problem of action selection for the target-driven visual navigation in unknown environments, the goal of which is to rapidly navigate from a random starting location in a scene to a specified target.

Relationship to Contemporary Work. There is extensive literature on learning a dynamics model, and using this model to train a policy. Most notable among these is the work from [29] that proposes the Imagination-Augmented Agent, which learns approximate environment models before outputting the action policy. Pascanu et al. [26] propose Imagination-based Planner, which can perform a variable number of imagination steps before any action. Ha et al. [12] incorporate a generative recurrent model into reinforcement learning to predict the future given the past in an unsupervised manner. However, the goal information is hard-coded in these neural networks and the experimental environments are generally simple and fully observed, leading to poor generalization to complex, high-dimensional tasks with unseen targets in partially observed scenes. Pathak et al. [27] learn an inverse dynamics model based on the demonstrated trajectory way-points from the expert and demonstrate navigation in previously unseen office environments with a TurtleBot. Although sharing a similar spirit, our work is different from this work. First, we learn the forward dynamics using a variational generative model, which explicitly models uncertainty over the visual observations compared to the deterministic process in [27]. Second, our action policy is directly based on the generated future, while their predicted action is used for inferring the future. We design the model with bidirectional information flowing to maximize the mutual information between the action and the adjacent observation pair.

3 Target-Driven Visual Navigation

In this section, we begin by outlining the target-driven visual navigation task. We then present our network, which combines an information theoretic regularization with deep reinforcement learning for this task.

3.1 Navigation Task Setup

We focus on learning a policy for navigating an agent from its current location to a target in an unknown scene using only visual observations. Our navigation problem is: given a target image g , at each time step t , the agent receives as input the first-person view of the environment x_t to predict the action a_t that will navigate the robot to the viewpoint where the target image g is taken.

Datasets. We conduct our experiments on the AI2-THOR and AVD. AI2-THOR consists of 120 synthetic scenes in four categories: kitchen, living room, bedroom, and bathroom. Each category includes 30 scenes, 20 of which are used for training, 5 for validating, and 5 for testing, in accordance with [36]. AVD contains 14 different real-world houses (except for one office room), 8 of which are used for training, 3 for validating, and 3 for testing referring to [24].

Observations. In contrast to the work [44], which stacks four history frames as current inputs at each time step, we utilize four views (RGB images by default) with evenly distributed azimuth angles at each location for current observation x_t . The resolution of each view is $300 * 300$.

Targets. The navigation target is specified by an RGB image, which contains a goal object such as a dining table, a refrigerator, a sofa, a television, a chair, etc. *Please refer to the supplemental material for the training and testing goal objects.* Our model learns to analyze the relationship between the current observation and the target image, and hence we can show generalization to novel targets and scenes, both of which the agent has not previously encountered.

Actions. Each scene in our datasets is discretized into a grid-world navigation graph. The agent acts on these graphs and its action space is determined by the connectivity structures of these graphs as a discrete set: $\{move\ forward; move\ back; move\ left; move\ right; rotate\ ccw; rotate\ cw; stop\}$, as defined in [24]. These above make it easy to acquire a shortest action path of a target-driven navigation task (e.g., using A* algorithm). In this work, we will show how to incorporate the shortest paths during training to learn a navigation controller.

Rewards. Our purpose during policy training is to minimize the trajectory length to the navigation targets. Therefore, reaching the target is assigned high values of reward 10.0 and we penalize each step with a small negative reward -0.01 . To avoid collision, we design a penalty -0.2 when hitting obstacles during run-time. In addition, we consider the geodesic distance to the goal at each time step, $Geo(x_t; g)$, as in [10] and reformulate the reward as:

$$r_t = \begin{cases} -0.01 & \text{if } t = 0 \\ +10.0 & \text{elif } succeed \\ -0.2 & \text{elif } collide \\ Geo(x_{t-1}, g) - Geo(x_t, g) - 0.01 & \text{otherwise.} \end{cases} \quad (1)$$

Success measure. In our setting, the navigation agent runs up to 100 steps, unless a stop action is issued or the task is successful. A navigation task is considered successful if the agent predicts a stop action, and the goal object is in the field of the current front-view, and the distance between the current location and the target view location is within a threshold of $0.5m$.

3.2 Information-theoretic Regularization

We formulate the target-driven visual navigation using a deep reinforcement learning framework (TD-A3C). At each time step t , the network takes the current observation x_t and the navigation target g as inputs and finally outputs an action distribution $\pi(x_t, g)$ and a scalar $v(x_t, g)$. We choose action a_t from the policy $\pi(x_t, g)$ and $v(x_t, g)$ is the value of the current policy. This network can be updated by minimizing a traditional RL navigation loss as in [44], which uses different policy networks for different scenes. Figure 1(a) shows the interaction between the agent and an environment. However, achieving strong results with one single policy network for all training scenes is difficult, since the agent is very

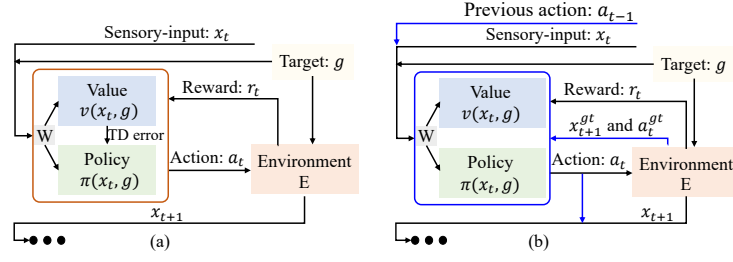


Fig. 1. Target-driven navigation flow diagram showing how agents interact with the environment. (a) Traditional RL agent (in the orange square). (b) Our agent (in the blue square). Layer parameters in a gray square are shared by a policy network and a value network. The blue represents the difference between the two flow diagrams. We propose using an information-theoretic regularization to facilitate the traditional RL learning, which requires more information from the environment, e.g., x_{t+1}^{gt} and a_t^{gt} .

sensitive to the RL reward function and requires extensive training time. In addition, [44] does not consider generalization to previously unseen environments, which are new houses with different layouts and furniture locations.

In order to address the shortcoming above, we revisit Shannon’s mutual information (MI) measure to further reduce the uncertainty in navigation action decision when visual observation is given. In navigation, let x_t denote the current observation, x_{t+1} denote the next observation, and a_t be the relative action between the two observations. We observe that a navigation agent always abides by an information-theoretic regularization: there should be high mutual information between the action a_t and the adjacent observation pair (x_t, x_{t+1}) , a joint variable. The mutual information $I(a_t; (x_t, x_{t+1}))$ is defined as:

$$\begin{aligned}
 I(a_t; (x_t, x_{t+1})) &= H(a_t) - H(a_t | x_t, x_{t+1}) \\
 &= \int p(a_t, x_t, x_{t+1}) \log p(a_t | x_t, x_{t+1}) da_t dx_t dx_{t+1} + H(a_t) \\
 &= \int p(x_{t+1} | x_t, a_t) p(x_t) p(a_t) \log p(a_t | x_t, x_{t+1}) da_t dx_t dx_{t+1} + H(a_t) \\
 &= \int p(x_{t+1} | z) p(z | x_t, a_t) p(x_t) p(a_t) \log p(a_t | x_t, x_{t+1}) da_t dx_t dx_{t+1} dz + H(a_t) \\
 &= E_{x_t \sim p(x_t)} [E_{x_{t+1} \sim p(x_{t+1} | z)} [E_{z \sim p(z | x_t, a_t)} [E_{a_t \sim p(a_t)} [\log p(a_t | x_t, x_{t+1})]]]] + H(a_t)
 \end{aligned} \tag{2}$$

We assume $a_t \sim \text{Cat}(1/C)$ since the navigation action space is a discrete set and hence $H(a_t)$ is a constant. This regularization provides a well-grounded action-observation dynamic model $p(x_{t+1} | x_t, a_t)$ and describes the causality between navigation actions and observational changes $p(a_t | x_t, x_{t+1})$. An agent that seeks to maximize this value will gain a compelling understanding of the dynamics and the causality. It is this intuition that leads us to incorporate the regularization into the target-driven navigation learning.

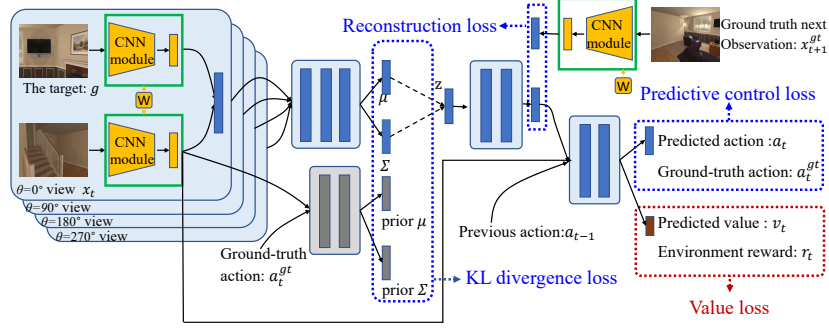


Fig. 2. Model overview. Our model integrates an information-theoretic regularization into an RL framework to constrain the intermediate process of the navigation policy. During training, our network is supervised by the environment reward r_t and the shortest path of the task in the form of the ground truth action a_t^{gt} and the ground truth next observation x_{t+1}^{gt} . The parameters are updated by four loss terms: the reconstruction, the KL, the predictive control and the value. The first three terms in blue are introduced by the information-theoretic regularization. At test time, the parameters are fixed and our network first takes the current observation and the target as inputs to generate the future state. Then it predicts the action based on the future and the current states. Layer parameters in the green squares are shared.

We propose adapting the task-independent regularization above by incorporating some supervision to help learn a strong target-driven visual navigation model. The supervision is from the shortest paths of target-driven navigation tasks. Specifically, at each time step, given the current observation and the target, the optimal next observation x_{t+1}^{gt} and relative action a_t^{gt} are provided as ground truth, see Figure 1(b). Over Equation 2, we first want the generative module $z \sim p(z|x_t, a_t)$, $x_{t+1} \sim p(x_{t+1}|z)$ to generate a next observation x_{t+1} , which is most related to the navigation task. Hence, we use the ground truth action a_t^{gt} to guide the generation: $z \sim p(z|x_t, a_t^{gt})$, $x_{t+1} \sim p(x_{t+1}|z)$ and use the ground truth x_{t+1}^{gt} to help update the generation module through a reconstruction term. Subsequently, the action prediction module $a_t \sim p(a_t|x_t, x_{t+1})$ is supervised by the ground truth action a_t^{gt} and hence is updated by a predictive control term. In addition, considering that a_t^{gt} is unknown a priori during real navigation and is inherently determined by the navigation target g , we design the distribution $q(z|x_t, g)$ to approximate the distribution $p(z|x_t, a_t^{gt})$. $z \sim p(z|x_t, a_t^{gt})$, $x_{t+1} \sim p(x_{t+1}|z)$ and $z \sim q(z|x_t, g)$ constitute our variational auto-encoder module. Overall, we obtain a lower bound of Equation 2 as:

$$\begin{aligned} \mathcal{J}(a_t, x_t, x_{t+1}) = & \alpha E_{z \sim q(z|x_t, g)} [\log p(x_{t+1}|z)] - \beta \mathcal{KL}[q(z|x_t, g) || \\ & p(z|a_t^{gt}, x_t)] + \gamma E_{a_t^{gt} \sim p(a_t^{gt})} [\log p(a_t|x_t, x_{t+1})] \end{aligned} \quad (3)$$

The hyper-parameter (α, β, γ) tunes the relative importance of the three terms: reconstruction, KL, and predictive control.

3.3 Regularized Navigation Model

The key idea in reinforcement learning for navigation is finding a policy $\pi(x_t, g)$ that can maximize expected future return. Within our regularized navigation framework, along with environment reward, our agent puts much attention on the ability to understand the action-observation dynamics and the causality between navigation actions and observational changes as well. This changes the RL problem to:

$$\pi^* = \arg \max_{\pi} E\left[\sum_{t=0}^{\infty} \tau^t r_t + \mathcal{J}(a_t, x_t, x_{t+1})\right] \quad (4)$$

where r_t is a reactive reward to the agent provided by the environment at each time step and $\tau \in (0, 1]$ is a discount factor. Corresponding to the above objective, we develop a new deep actor-critic network, see Figure 2.

Policy Network. The inputs to the policy network are the multi-view images x_t and the target image g at each time step t . The network first learns to reason about some important information from the current observation based on the target, which is then used for generating the next expected observation. This process is supervised by the action-observation dynamics $p(x_{t+1}|x_t, a_t^{gt})$ and the ground truth next observation x_{t+1}^{gt} . Information from the generated observation and the current observation is fused to form a joint representation, which is passed through the predictive control layer for predict the navigation action.

In addition, we investigate two techniques to improve the training performance. First, we find that when the previous action a_{t-1} is provided, the agent is less likely to move or rotate back and forth in a scene. This is reasonable since the ground truth action has no chance to be in contradiction with the previous action (e.g., move forward vs move backward). Second, we apply a CNN module f to derive a state representation from an image and hence get the current state $f(x_t)$, the ground truth next state $f(x_{t+1}^{gt})$, and the goal state $f(g)$. In our work, we do not directly generate the next observation x_{t+1} . We generate the state representation, denoted as $s_{t+1} \sim p(s_{t+1}|z)$ and use this to compute the reconstruction loss and predict the navigation action. To avoid confusions, we will still use the description of generating the next observation below. This simplification reduces the network parameters and hence computational cost. As a result, our navigation policy is updated by:

$$\begin{aligned} \mathcal{L}_p = & \alpha \text{MSE}(s_{t+1}, f(x_{t+1}^{gt})) + \beta \mathcal{KL}[q(z|f(x_t), f(g))||p(z|a_t^{gt}, f(x_t))] \\ & + \gamma E_{a_t^{gt} \sim p(a_t^{gt})}[-\log p(a_t|f(x_t), s_{t+1}, a_{t-1})] \end{aligned} \quad (5)$$

Value Network. We learn a value function from the penultimate fully connected layer of our policy $\pi(x_t, g)$, which represents the value of the current policy at the current navigation task, denoted as $v(x_t, g)$. This is associated with a value loss $\mathcal{L}_v = E_{x_t, r_t}[(R_t - v(x_t, g))^2]$, where R_t is the discounted accumulative reward defined by $R_t = \sum_{i=0}^{T-t} \tau^i r_{t+i} + v(x_{T+1}, g)$. Unlike previous work [44] which directly uses the value $v(x_t, g)$ (embodied as a TD error) to help

update the navigation policy, see Figure 1(a), our value term \mathcal{L}_v merely affects the shared layers of the policy in Figure 1(b).

Therefore, the overall loss function is $\mathcal{L} = \mathcal{L}_p + \omega\mathcal{L}_v$, where the hyperparameter is empirically set as ($\alpha = 0.1$, $\beta = 0.0001$, $\gamma = 1$, $\omega = 0.5$) throughout our experiments. *Please refer to the supplemental material for more details.*

At test time, three modules $z \sim q(z|x_t, g)$, $x_{t+1} \sim p(x_{t+1}|z)$ and $a_t \sim p(a_t|x_t, x_{t+1}, a_{t-1})$ constitute our controller for the agent to predict the next action given the current observation, the target view and the previous action. The controller can navigate robots in unseen scenes, of which the environment maps (graphs) are not known.

4 Implementation and Performance

Our main objective is to improve the cross-target and cross-scene generalization of target-driven navigation. In this section, we evaluate our navigation model compared to baselines based on standard deep RL models and/or traditional imitation learning. We also provide ablation results to gain insight into how performance is affected by changing the structures in our model.

4.1 Baselines and Ablations

We compare with the following navigation models:

- **Random Walk** randomly draws a navigation action at each time step.
- **TD-A3C** is the target-driven visual navigation model from [44]. It is trained using standard reinforcement learning, but it has the same action space and reward function as ours, and uses previous action to assist the policy learning.
- **TD-A3C(BC)** is a variation of the TD-A3C. It is trained using behavioral cloning (BC), where the policy is supervised by shortest paths. The CNN module is the same as ours. The main difference to ours lies in how to exploit the supervision information.
- **Gated-LSTM-A3C(BC)** is an LSTM-based variant of A3C model adapted from [37], which is trained with BC and provided with previous action. The goal is specified as an image.
- **TD-Semantic** is a navigation model from [24]. The method predicts the cost of an action, which is supervised by shortest paths of navigation tasks.
- **Ours-FroView** is a variant of ours and takes the current front-view to generate the future rather than the four views around the agent location.
- **Ours-NoGen** is a variation of our model, which predicts the observation from the current observation and the target without a stochastic latent space.
- **Ours-VallinaGen** is a variant of ours, in which the latent space $z \sim q(z|x_t, g)$ is constrained by the standard normal distribution prior $p(z)$.

We train and evaluate all these models on the two datasets described in Section 3.1. *More implementation details are provided in the supplemental material.*

Table 1. Average navigation performance (SR and SPL in %) comparisons on unseen scenes from AI2-THOR with stop action and without stop action, respectively.

		With Stop Action				Without Stop Action			
		All		$L \geq 5$		All		$L \geq 5$	
		SR	SPL	SR	SPL	SR	SPL	SR	SPL
Unseen scenes, Known targets P=17.7%	Random	1.2	0.7	0.6	0.3	28.9	3.2	21.3	1.9
	TD-A3C	20.0	4.0	12.9	2.6	32.4	10.2	27.1	9.8
	TD-A3C(BC)	23.0	7.9	13.4	3.7	35.9	12.4	31.3	10.1
	Gated-LSTM-A3C(BC)	29.1	10.5	19.2	5.1	40.3	16.3	35.1	11.4
	Ours	45.7	25.8	41.9	24.8	47.3	31.5	42.6	27.7
	Ours-FroView	32.3	10.3	29.8	9.4	46.2	17.7	40.1	14.2
	Ours-NoGen	41.2	23.8	38.5	22.2	47.1	30.9	41.9	28.1
	Ours-VallinaGen	37.5	17.7	34.0	15.9	45.5	28.9	40.7	27.3
Unseen scenes, Novel targets P=16.0%	Random	2.0	1.0	0.6	0.4	27.3	4.1	22.3	2.2
	TD-A3C	10.1	1.9	6.3	1.1	30.4	11.9	26.9	8.2
	TD-A3C(BC)	12.3	2.4	7.5	1.6	31.7	10.3	26.9	8.7
	Gated-LSTM-A3C(BC)	30.0	11.4	26.7	8.6	36.1	14.3	32.3	10.1
	Ours	37.7	20.5	35.4	19.7	41.6	27.2	38.8	25.1
	Ours-FroView	24.6	7.8	23.0	6.9	39.7	16.8	37.1	14.2
	Ours-NoGen	35.7	19.1	31.6	17.4	40.8	22.0	37.2	19.2
	Ours-VallinaGen	31.4	13.9	29.4	12.7	35.9	17.9	32.4	15.9

4.2 Evaluation Details

The evaluation is divided into two different levels on our testing set, $\{Unseen\ scenes, Known\ targets\}$ and $\{Unseen\ scenes, Novel\ targets\}$. Each level evaluation contains 1000 different navigation tasks. [33] proposes using the ratio of the shortest path distance to the Euclidean distance between start and goal positions, to benchmark navigation task difficulty. In each evaluation, we compute the percentage P of the tasks that have a ratio within the range of $[1, 1.1]$ and evaluate the performance on all tasks and on tasks where the optimal path length L is at least 5. We evaluate these models on two metrics, success rate (SR) and success weighted by (normalized inverse) path length (SPL) as defined in [39].

4.3 Results on the AI2-THOR

Generalization. We analyze the cross-target and cross-scene generalization ability of these models on AI2-THOR. Table 6 summarizes the results. First, we observe a higher generalization performance for the model with supervision comparing the results from TD-A3C and TD-A3C(BC). We believe that it is more challenging for RL networks to discover the optimal outputs in the higher-order control tasks. In addition, pretraining on ImageNet (TD-A3C) does not offer better generalization, since the features required for ImageNet are different from those needed for navigation. Subsequently, considering the navigation performance difference between TD-A3C(BC) and Ours (or Ours-FroView), we see that the idea of generating the future before acting and acting based on the visual difference, works better than directly learning a mapping from raw images to a navigation action. We also compare to Gated-LSTM-A3C(BC), which

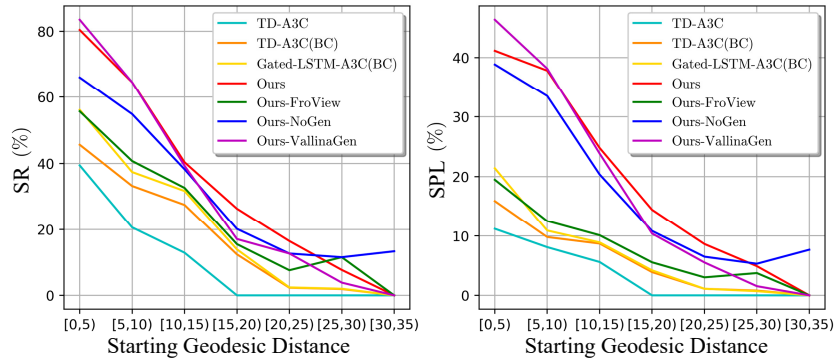


Fig. 3. We report SR and SPL performance as a function of starting geodesic distance from the target.

uses an LSTM based memory and has access to shortest paths during training as we do. Our model is able to consistently outperform the LSTM based baseline. These above show that the proposed information-theoretic regularization effectively brings us better generalization for unseen scenes and novel objects.

Ablation. The ablation on different inputs (Front-view vs Multi-view) demonstrates that it is easier to generate the next observation, when the current information is rich. We also conduct the ablation with four history frames as current inputs, which is difficult to converge in training scenes. We consider that there is no direct connection between the random history and the next observation, which is most related to the current observation and the target. Hence, it is more reasonable to generate the future from the current multi-view observation rather than the history. Based on the ablation on the generation process, we conclude that learning a stochastic latent space is often more generalizable than learning a deterministic one (Ours vs Ours-NoGen), since the former explicitly models the uncertainty over visual images. This is in accordance with the work from [3]. However, when the latent space is over-regularized by the standard normal distribution prior, the situation is worse (Ours-VallinaGen vs Ours).

Termination criterion. It is difficult for a navigation agent to learn to issue a stop action at a correct location, since there is only one situation with stop action but many cases with other actions during a navigation task. Table 6(right) shows a simpler case where the stop signal is provided by the environment rather than being predicted by an agent. As expected, all models demonstrate higher performances than Table 6(left). Additionally, we see the performance gap of our model is much smaller than the alternatives, meaning we handle the data imbalance better than the baselines. We attribute the good performance to the natural design of the regularization in our model. The regularization models the environment dynamics and the causality between navigation actions and observational changes, embodied as $p(x_{t+1}|x_t, a_t)$ and $p(a_t|x_t, x_t + 1)$, respectively. This motivates an agent to focus more on learning the ability of understanding navigation tasks than maximizing long-term returns.

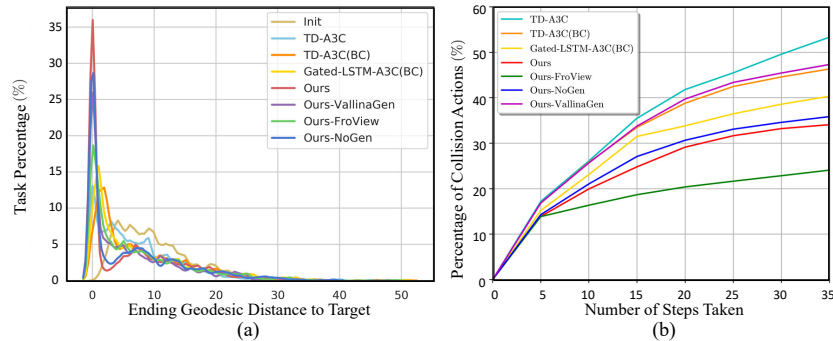


Fig. 4. Analysis. (a) We fit the ending geodesic distance distribution of all learning models over 1000 navigation tasks. The Init represents the starting geodesic distance distribution of these tasks. (b) We report the collision action percentages of all learning models as the navigation proceeds.

Geodesic distance. We further analyze the navigation performance (SR and SPL) as a function of the geodesic distance between the start and the target locations in Figure 3. This is based on the 1000 navigation tasks from the $\{Unseen\ scenes, Known\ targets\}$ evaluation. As can be seen, the geodesic distance is highly correlated with the difficulty of navigation tasks and the performance of all methods degrades as the distance between the start and the target increases. Our model outperforms all alternatives in most cases. Most notable thing is all methods but one (Ours-NoGen) fail in these navigation tasks, of which the geodesic distances fall into $[30, 35)$. It is possible for Ours-NoGen performs better than other methods on this evaluation, since the test scenes are small and just a few navigation tasks fall into the $[30, 35)$ interval. We also provide the statistics of geodesic distance to the target locations of all the compared models after navigation. As illustrated by Figure 4(a), all learning models experience a decrease in the average distance to the targets, demonstrating the effectiveness of learning compared to the initial geodesic distance distribution of these evaluated navigation tasks.

Collisions. We assume a collision detection module is devised and when a collision is detected, an agent will stay and make a new action decision. In this case, two outcomes can be expected: 1) the action from the policy distribution can help the agent get out of the dilemma; 2) the action is equal to the old action and the agent gets stuck until the maximum number of steps (100) is reached and finally fails the task. We evaluate 1000 trajectories from Figure 3 by computing the ratio of collisions as the navigation proceeds. As shown in Figure 4(b), the ablated model, Ours-FroView, presents the best performance. We consider that rich visual information maybe against the collision avoidance, since it is challenging for a robot to extract some useful cues for both shortest navigation and avoiding collisions. Overall, our model can deal with collisions more properly than the baselines as the navigation progresses.

Table 2. Average navigation performance (SR and SPL in %) comparisons on unseen scenes from AVD.

		Table	Exit	Couch	Refrigerator	Sink	Avg.
With Stop Action	Random	4.0 / 2.7	4.6 / 3.1	3.4 / 2.1	3.2 / 2.1	3.6 / 2.7	3.8 / 2.7
	TD-A3C	7.4 / 2.9	6.9 / 4.0	5.7 / 3.6	6.1 / 3.3	5.9 / 3.2	6.4 / 3.4
	TD-A3C(BC)	22.6 / 13.4	8.6 / 3.0	10.0 / 2.6	17.8 / 8.1	14.2 / 6.0	14.6 / 6.6
	Gated-LSTM-A3C(BC)	16.4 / 7.3	8.4 / 2.6	15.0 / 6.9	15.2 / 6.2	7.0 / 2.1	12.4 / 5.0
	Ours	23.4 / 8.5	10.1 / 5.3	31.9 / 13.1	18.9 / 3.5	25.7 / 7.0	22.0 / 7.5
Without Stop Action	Random	34.8 / 12.9	29.0 / 11.3	29.8 / 10.8	27.4 / 10.7	23.0 / 10.2	28.8 / 11.2
	TD-A3C	37.9 / 13.4	34.3 / 11.2	31.9 / 10.3	32.6 / 12.4	23.7 / 9.1	32.1 / 11.3
	TD-A3C(BC)	36.0 / 22.4	33.6 / 14.8	27.6 / 11.8	59.8 / 24.8	51.6 / 25.7	41.7 / 19.9
	Gated-LSTM-A3C(BC)	28.2 / 12.2	32.2 / 13.6	39.4 / 15.0	33.6 / 14.8	37.6 / 15.7	34.2 / 14.3
	Ours	61.9 / 35.0	56.7 / 28.1	65.7 / 27.5	40.1 / 16.9	50.6 / 20.1	55.0 / 25.5

Table 3. Performance (SR) comparison of semantic navigation on the AVD test split.

Target label	Couch	Table	Refrigerator	Microwave	TV	Avg.
TD-Semantic (Object)	80.0	38.0	68.0	38.0	44.0	53.6
Ours (RGB)	71.2	62.6	51.0	41.2	39.6	53.1
Ours (Depth)	67.0	81.2	61.4	49.6	35.8	59.0

4.4 Results on the AVD

Generalization. To evaluate the generalization ability in the real world, we train and evaluate our model and three alternatives based on the training and testing splits on AVD. All methods being compared take depth input with the resolution of $64 * 64$. We relax the criterion for successful navigation (the stop action should be issued, the distance of the agent to the target position is less than 1 meter and the angle between the current and target view direction is less than 90°). We present the results in Table 7, which is based on 1000 navigation tasks ($P = 15.0\%$) randomly sampled from the test scenes on AVD. We observe that all four learning models demonstrate average performance decreases compared to the results with stop action on AI2-THOR in Table 6. Additionally, we see a large gap between the performances of all compared models with stop action and without stop action, since the AVD dataset is small and the navigation targets on it are limited in our setting. This results in a severe data imbalance. These models all have difficulty in issuing a correct stop action. Most notably, our method exhibits significant robustness towards the real world with at least 7.4% absolute improvement in success rate over the TD-A3C(BC) baseline.

Navigation driven by semantic labels. We adapt our method to compare with TD-Semantic [24], in which the navigation goal is defined in the form of a one-hot vector over a prescribed set of semantic labels, $\{Couch; Table; Refrigerator; Microwave; TV\}$. The experiment is conducted on AVD with the same training/testing split and success criterion as [24]. While sharing the same idea of improving the training by using the supervision from shortest paths of navigation tasks, our method outperforms TD-Semantic by 22% for RGB input (53% vs 31%), and 28% for depth input (59% vs 31%) for average success rate on AVD testing set. The best performances of two methods over various target labels are presented in Table 3. Our method (with depth input) shows 5.4%

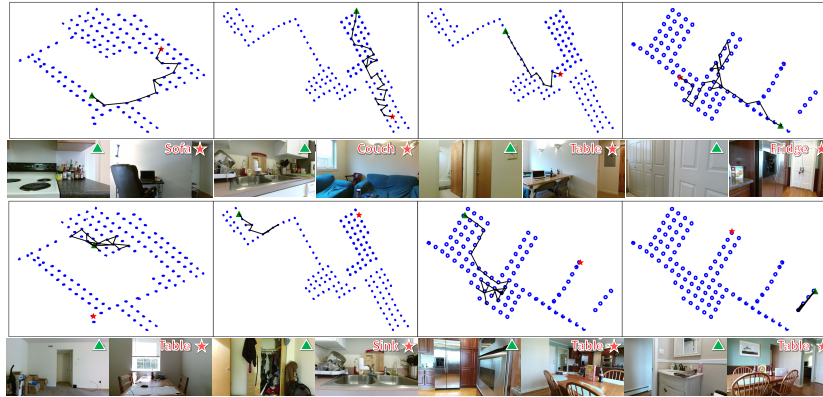


Fig. 5. Visualization of some typical success and failure cases of our method in eight navigation tasks from AVD. The blue dots represent reachable locations in the scene. Green triangles and red stars denote starting and goal points, respectively.

improvement in average success rate compared to TD-Semantic with semantic input, which is provided by some state-of-the-art detectors and segmentors. We consider our information-theoretic regularization helps learn a controller which can analyze the relation between visual observation and the target and then extract some important information to guide the navigation. This process is not affected by the target format, e.g., a semantic label or a view image.

Visualization. We visualize eight navigation trajectories from our model in Figure 5. These tasks are all characterized by unknown scenes, and long distances between the start points and the targets. For the tasks in the first row, our agent is able to navigate to the targets successfully, but for the last four tasks, our model fails to finish within the maximum number of steps. The problems include thrashing around in space without making progress (see the first and third trajectories in the second row), getting stuck in the corridor (see the second trajectory in the second row), and navigating around tight spaces (e.g, the small bathroom where the fourth trajectory starts).

5 Conclusion

We propose integrating an information-theoretic regularization into a deep reinforcement learning framework for the target-driven task of visual navigation. The regularization maximizes the mutual information between navigation action and visual observations, which essentially models the action-observation dynamics and the causality between navigation actions and observational changes. By adapting the regularization for target-driven navigation, our agent further learns to build the correlation between the observation and the target. The experiments show that our model outperforms some supervised baselines by a large margin in both the cross-scene and the cross-target generalization during navigation.

Table 4. Training and testing split of object classes over scene categories of AI2-THOR.

Room type	Train objects	Test objects
Kitchen	Toaster, Microwave, Fridge, CoffeeMaker, GarbageCan, Box, Bowl, Apple, Chair, DiningTable, Plate, Sink, SinkBasin	StoveBurner, Cabinet, HousePlant
Living room	Pillow, Laptop, Television, GarbageCan, Box, Bowl, Book, FloorLamp, Sofa	Statue, TableTop, HousePlant
Bedroom	Lamp, Book, AlarmClock, Bed, Mirror, Pillow, GarbageCan, TissueBox,	Cabinet, Statue, Dresser, LightSwitch
Bathroom	Sink, ToiletPaper, SoapBottle, LightSwitch, Candle, GarbageCan, SinkBasin, ScrubBrush	Cabinet, Towel, TowelHolder

The current navigation policy is still sensitive to the data imbalance when the training task set is limited (see the large performance gap in Table 7). In the future, we plan to exploit some high level semantic and contextual features to facilitate the understanding of navigation tasks and learn more robust navigation strategies with limited training set to apply to some real-world scenarios.

6 Appendix

6.1 Navigation Targets

Our navigation targets are specified by images, which contain goal objects, such as dining tables, refrigerators, sofas, televisions, chairs, etc. AI2-THOR provides all visible RGB views for each goal object. These views are collected based on three conditions. First, the view should be from the camera’s viewport. Second, the goal object should be within a threshold of distance from the agent’s center (1.5m by default). Third, a ray emitted from the camera should hit the object without first hitting another obstruction. In our experiments on AI2-THOR, we have access to about 18,231 different target views from 80 training scenes for training. In Table 4, we provide the split of object classes used in the training and testing processes of all learning models. For AVD, we manually select 120 target views in depth from the training split (8 scenes), including some common objects as $\{Couch, Table, Fridge, Microwave, Sink, TV, Cabinet, Toaster, GarbageCan, Door, Chair, Bed, Dresser, Mirror\}$.

6.2 Network Architecture

Our CNN module for deriving a state representation from an image is presented in Figure 6(a). By default, spectral normalization is used for the first six layers, which can prevent the escalation of parameter magnitudes and avoid unusual gradients [21,41]. The activation function used is LeakyReLU (0.1). At each time step t , we take the four-view observation x_t as well as the target g as inputs and extract a 512-D state vector for each of them. We concatenate each view state with the target state to get a fused feature (see Figure 6(b)). In Figure 6(d), four feature vectors are then used to infer a vector of latent variables of dimension 512 with a MLP. Here, a KL divergence loss is minimized to impose the distribution of the latent variables to match a prior distribution $p(z|x_t, a_t^{gt})$

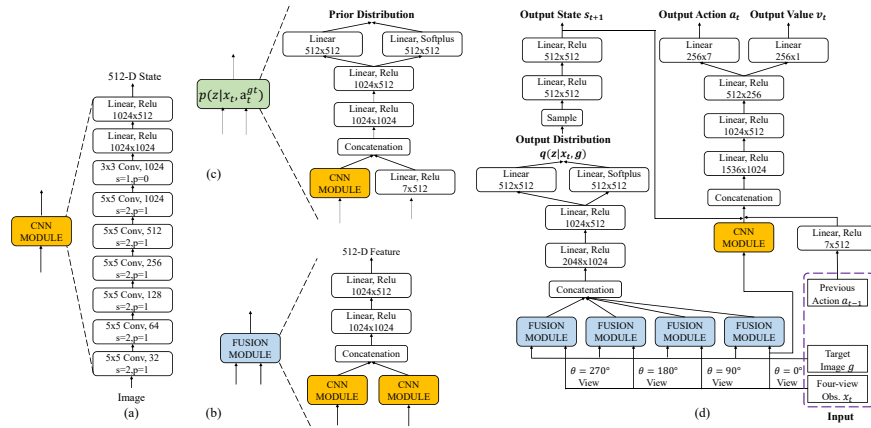


Fig. 6. Model architecture. The overview is given (d) with blowups of (a) the CNN module (the orange portion), (b) the fusion module (the blue portion) and (d) the prior distribution (the green portion).

from Figure 6(c), which is estimated from the current observation x_t (front view only) and the ground-truth action a_t^{gt} . The latent vector $z \sim q(z|x_t, g)$ is used to generate a state s_{t+1} of next observation, which is under the supervision of ground truth next observation x_{t+1}^{gt} . Subsequently, the generated state s_{t+1} of next observation (512-D), the state of front view observation (512-D), and the feature (512-D) extracted from the previous action a_{t-1} (7-D one-hot vector) are combined together to predict the navigation action a_t (7-D) and get the evaluation value v_t (1-D). The ground-truth action a_t^{gt} and environment reward r_t are used to help update this module.

6.3 Implementation Details

We train our model using 6 asynchronous workers and then back-propagate through time for every 10 unrolled time steps. The batch size is 60 for each back-propagation. We use RMSprop optimizer to update the network parameters with a learning rate of $1e^{-4}$ and a smoothing constant of 0.99. Our model is trained and tested on a PC with 12 Intel(R) Xeon(R) W-2133 CPU, 3.60 GHz and a Geforce GTX 1080 Ti GPU. The training configurations of our ablation models and alternatives, including TD-A3C, TD-A3C(BC), Gated-LSTM-A3C(BC), are much the same as ours. For all compared models, training on AI2-THOR is carried out in four stages, starting with 20 kitchens, to gradually increase by 20 scenes (namely, a scene category) at each next stage. This ensures fast convergence in training scenes. Training on 8 scenes from AVD for all learning models is continuous. The training time of our model is about 24 hours on 8 scenes of AVD and 120 hours on 80 scenes of AI2-THOR. We take the model for evaluation which performs best on the validation set.

Table 5. Comparing navigation performance (SR and SPL in %) on different scene categories on AI2-THOR with stop action.

Category	Kitchen P=15.2%	Living room P=15.6%	Bedroom P=20.0%	Bathroom P=20.0%
Random	0.0 / 0.0	1.6 / 1.0	2.0 / 1.1	1.2 / 0.7
TD-A3C	17.4 / 3.1	13.2 / 2.1	16.9 / 1.9	32.4 / 9.0
TD-A3C(BC)	21.3 / 7.8	18.2 / 5.2	22.4 / 8.1	30.1 / 10.4
Gated-LSTM-A3C(BC)	28.2 / 10.9	23.6 / 7.2	28.0 / 10.4	36.6 / 13.4
Ours	42.6 / 23.6	36.7 / 19.6	40.6 / 21.8	62.7 / 38.1
Ours-FroView	34.8 / 11.2	17.6 / 5.0	28.0 / 9.2	48.8 / 16.0
Ours-NoGen	38.8 / 22.0	28.8 / 15.4	38.8 / 22.7	58.4 / 35.2
Ours-VallinaGen	47.2 / 24.0	15.6 / 6.1	34.8 / 13.5	52.4 / 27.3

6.4 Additional Results

Scene category. Table 5 presents the navigation performance on different scene categories, which is based on the $\{Unseen\ scenes, Known\ targets\}$ evaluation tasks from AI2-THOR in the main paper. All methods consistently demonstrate impressive navigation performance in small scenes, e.g., kitchen and bathroom. However, navigation in large rooms, e.g., living room, is much more challenging.

Input modality. We conduct additional experiments of our method, where using semantic segmented images from AI2-THOR as inputs. The training and testing setting is the same as the main paper. In Table 6, all navigation tasks are from the evaluation of generalization on AI2-THOR in the main paper. Although semantic segmented images are lossy compared to RGB, they do capture most of the important information for navigation, leading to substantial navigation performance improvement as expected.

Table 6. Navigation performance (SR and SPL in %) on different input modalities from AI2-THOR with stop action.

	Category	Kitchen P=15.2%	Living room P=15.6%	Bedroom P=20.0%	Bathroom P=20.0%	Avg. P=17.7%
Cross -scene	Random	0.0 / 0.0	1.6 / 1.0	2.0 / 1.1	1.2 / 0.7	1.2 / 0.7
	Ours(RGB)	42.6 / 23.6	36.7 / 19.6	40.6 / 21.8	62.7 / 38.1	45.7 / 25.8
	Ours(Semantic)	58.4 / 39.0	25.4 / 14.5	44.4 / 23.3	61.6 / 39.5	47.5 / 29.1
	Category	Kitchen P=20.0%	Living room P=13.6%	Bedroom P=15.6%	Bathroom P=14.6%	Avg. P=16.0%
Cross -target	Random	2.8 / 1.4	0.4 / 0.1	1.6 / 0.1	3.2 / 1.5	2.0 / 1.0
	Ours(RGB)	46.6 / 26.1	22.6 / 9.4	39.0 / 21.1	42.6 / 25.4	37.7 / 20.5
	Ours(Semantic)	53.6 / 34.8	22.4 / 10.3	43.2 / 23.1	47.6 / 27.8	41.7 / 24.0

Navigation comparison on AVD RGB input. We further compare the navigation performances of all methods, where using RGB images from AVD as inputs. The input image resolution is $64 * 64$. In Table 7, all navigation tasks are

from the evaluation of cross-scene generalization on AVD in the main paper. Our model suffers from more performance degrading compared to the default depth input than other learning alternatives. We consider depth images contain rich spatial information for reasoning about the surroundings, which is particularly important in our visual navigation.

Table 7. Average navigation performance (SR and SPL in %) comparisons on unseen scenes from AVD (RGB).

		Table	Exit	Couch	Refrigerator	Sink	Avg.
With Stop Action	Random	4.0 / 2.7	4.6 / 3.1	3.4 / 2.1	3.2 / 2.1	3.6 / 2.7	3.8 / 2.7
	TD-A3C	7.0 / 3.4	5.7 / 2.6	6.3 / 3.1	7.5 / 4.1	7.9 / 3.7	6.9 / 3.4
	TD-A3C(BC)	6.4 / 3.8	3.4 / 1.0	19.4 / 7.0	13.6 / 5.6	14.0 / 5.5	11.4 / 4.6
	Gated-LSTM-A3C(BC)	6.2 / 3.0	8.9 / 3.1	14.8 / 6.9	13.7 / 6.1	10.3 / 5.7	10.8 / 5.0
	Ours	9.2 / 6.9	20.0 / 10.4	15.4 / 8.6	9.0 / 7.7	11.0 / 8.8	12.9 / 8.5
Without Stop Action	Random	34.8 / 12.9	29.0 / 11.3	29.8 / 10.8	27.4 / 10.7	23.0 / 10.2	28.8 / 11.2
	TD-A3C	29.7 / 11.9	27.3 / 9.6	35.3 / 12.7	31.6 / 10.9	32.9 / 10.1	31.4 / 11.0
	TD-A3C(BC)	16.6 / 8.0	15.6 / 9.7	58.8 / 22.5	40.8 / 16.5	38.6 / 16.1	36.1 / 14.6
	Gated-LSTM-A3C(BC)	25.6 / 9.9	32.0 / 10.9	35.0 / 10.9	34.8 / 12.1	34.2 / 12.6	32.3 / 11.9
	Ours	42.2 / 20.3	36.2 / 14.2	39.4 / 13.8	24.2 / 11.6	43.4 / 18.7	37.1 / 15.7

References

1. Ammirato, P., Poirson, P., Park, E., Košecká, J., Berg, A.C.: A dataset for developing and benchmarking active vision. In: Proc. ICRA. pp. 1378–1385 (2017)
2. Bai, S., Wang, J., Chen, F., Englot, B.: Information-theoretic exploration with bayesian optimization. In: 2016 IEEE/RSJ International Conference on Intelligent Robots and Systems (IROS). pp. 1816–1822. IEEE (2016)
3. Buesing, L., Weber, T., Racaniere, S., Eslami, S., Rezende, D., Reichert, D.P., Viola, F., Besse, F., Gregor, K., Hassabis, D., et al.: Learning and querying fast generative models for reinforcement learning. arXiv preprint arXiv:1802.03006 (2018)
4. Charrow, B., Kahn, G., Patil, S., Liu, S., Goldberg, K., Abbeel, P., Michael, N., Kumar, V.: Information-theoretic planning with trajectory optimization for dense 3d mapping. In: Robotics: Science and Systems. vol. 11 (2015)
5. Chen, Y.F., Liu, M., Everett, M., How, J.P.: Decentralized non-communicating multiagent collision avoidance with deep reinforcement learning. In: Proc. ICRA. pp. 285–292 (2017)
6. Dame, A., Marchand, E.: Mutual information-based visual servoing. IEEE Transactions on Robotics **27**(5), 958–969 (2011)
7. Dosovitskiy, A., Koltun, V.: Learning to act by predicting the future. arXiv preprint arXiv:1611.01779 (2016)
8. Gao, Y., Lin, J., Yu, F., Levine, S., Darrell, T., et al.: Reinforcement learning from imperfect demonstrations. arXiv preprint arXiv:1802.05313 (2018)
9. Gimelfarb, M., Sanner, S., Lee, C.G.: Reinforcement learning with multiple experts: A bayesian model combination approach. In: Advances in Neural Information Processing Systems. pp. 9528–9538 (2018)
10. Gordon, D., Kadian, A., Parikh, D., Hoffman, J., Batra, D.: Splitnet: Sim2sim and task2task transfer for embodied visual navigation. arXiv preprint arXiv:1905.07512 (2019)

11. Gupta, S., Davidson, J., Levine, S., Sukthankar, R., Malik, J.: Cognitive mapping and planning for visual navigation. In: Proc. CVPR. pp. 2616–2625 (2017)
12. Ha, D., Schmidhuber, J.: Recurrent world models facilitate policy evolution. In: Advances in Neural Information Processing Systems. pp. 2450–2462 (2018)
13. Ho, J., Ermon, S.: Generative adversarial imitation learning. In: Advances in neural information processing systems. pp. 4565–4573 (2016)
14. Jaderberg, M., Mnih, V., Czarnecki, W.M., Schaul, T., Leibo, J.Z., Silver, D., Kavukcuoglu, K.: Reinforcement learning with unsupervised auxiliary tasks. arXiv preprint arXiv:1611.05397 (2016)
15. Kahn, G., Villafior, A., Ding, B., Abbeel, P., Levine, S.: Self-supervised deep reinforcement learning with generalized computation graphs for robot navigation. In: 2018 IEEE International Conference on Robotics and Automation (ICRA). pp. 1–8. IEEE (2018)
16. Li, G., Mueller, M., Casser, V., Smith, N., Michels, D.L., Ghanem, B.: Oil: Observational imitation learning. arXiv preprint arXiv:1803.01129 (2018)
17. Liang, X., Wang, T., Yang, L., Xing, E.: Cirl: Controllable imitative reinforcement learning for vision-based self-driving. In: Proceedings of the European Conference on Computer Vision (ECCV). pp. 584–599 (2018)
18. Liu, J., Gu, X., Zhang, D., Liu, S.: On-policy reinforcement learning with entropy regularization. arXiv preprint arXiv:1912.01557 (2019)
19. MartiNez, S., Bullo, F.: Optimal sensor placement and motion coordination for target tracking. *Automatica* **42**(4), 661–668 (2006)
20. Mirowski, P., Pascanu, R., Viola, F., Soyer, H., Ballard, A.J., Banino, A., Denil, M., Goroshin, R., Sifre, L., Kavukcuoglu, K., et al.: Learning to navigate in complex environments. arXiv preprint arXiv:1611.03673 (2016)
21. Miyato, T., Kataoka, T., Koyama, M., Yoshida, Y.: Spectral normalization for generative adversarial networks. arXiv preprint arXiv:1802.05957 (2018)
22. Mnih, V., Badia, A.P., Mirza, M., Graves, A., Lillicrap, T., Harley, T., Silver, D., Kavukcuoglu, K.: Asynchronous methods for deep reinforcement learning. In: Proc. ICML. pp. 1928–1937 (2016)
23. Mohamed, S., Rezende, D.J.: Variational information maximisation for intrinsically motivated reinforcement learning. In: Advances in neural information processing systems. pp. 2125–2133 (2015)
24. Mousavian, A., Toshev, A., Fišer, M., Košecká, J., Wahid, A., Davidson, J.: Visual representations for semantic target driven navigation. In: 2019 International Conference on Robotics and Automation (ICRA). pp. 8846–8852. IEEE (2019)
25. Muller, M., Li, G., Casser, V., Smith, N., Michels, D.L., Ghanem, B.: Learning a controller fusion network by online trajectory filtering for vision-based uav racing. In: Proceedings of the IEEE Conference on Computer Vision and Pattern Recognition Workshops. pp. 0–0 (2019)
26. Pascanu, R., Li, Y., Vinyals, O., Heess, N., Buesing, L., Racanière, S., Reichert, D., Weber, T., Wierstra, D., Battaglia, P.: Learning model-based planning from scratch. arXiv preprint arXiv:1707.06170 (2017)
27. Pathak, D., Mahmoudieh, P., Luo, G., Agrawal, P., Chen, D., Shentu, Y., Shihamer, E., Malik, J., Efros, A.A., Darrell, T.: Zero-shot visual imitation. In: Proceedings of the IEEE Conference on Computer Vision and Pattern Recognition Workshops. pp. 2050–2053 (2018)
28. Pomerleau, D.A.: *Neural Network Perception for Mobile Robot Guidance*. Kluwer Academic Publishers, Norwell, MA, USA (1993)

29. Racanière, S., Weber, T., Reichert, D., Buesing, L., Guez, A., Rezende, D.J., Badia, A.P., Vinyals, O., Heess, N., Li, Y., et al.: Imagination-augmented agents for deep reinforcement learning. In: *Advances in neural information processing systems*. pp. 5690–5701 (2017)
30. Rajeswaran, A., Kumar, V., Gupta, A., Vezzani, G., Schulman, J., Todorov, E., Levine, S.: Learning complex dexterous manipulation with deep reinforcement learning and demonstrations. *arXiv preprint arXiv:1709.10087* (2017)
31. Ross, S., Gordon, G., Bagnell, D.: A reduction of imitation learning and structured prediction to no-regret online learning. In: *Proceedings of the fourteenth international conference on artificial intelligence and statistics*. pp. 627–635 (2011)
32. Savinov, N., Dosovitskiy, A., Koltun, V.: Semi-parametric topological memory for navigation. *arXiv preprint arXiv:1803.00653* (2018)
33. Savva, M., Kadian, A., Maksymets, O., Zhao, Y., Wijmans, E., Jain, B., Straub, J., Liu, J., Koltun, V., Malik, J., et al.: Habitat: A platform for embodied ai research. *arXiv preprint arXiv:1904.01201* (2019)
34. Sun, W., Venkatraman, A., Gordon, G.J., Boots, B., Bagnell, J.A.: Deeply aggravated: Differentiable imitation learning for sequential prediction. In: *Proceedings of the 34th International Conference on Machine Learning-Volume 70*. pp. 3309–3318. JMLR. org (2017)
35. Taylor, M.E., Suay, H.B., Chernova, S.: Integrating reinforcement learning with human demonstrations of varying ability. In: *The 10th International Conference on Autonomous Agents and Multiagent Systems-Volume 2*. pp. 617–624. International Foundation for Autonomous Agents and Multiagent Systems (2011)
36. Wortsman, M., Ehsani, K., Rastegari, M., Farhadi, A., Mottaghi, R.: Learning to learn how to learn: Self-adaptive visual navigation using meta-learning. In: *Proceedings of the IEEE Conference on Computer Vision and Pattern Recognition*. pp. 6750–6759 (2019)
37. Wu, Y., Wu, Y., Gkioxari, G., Tian, Y.: Building generalizable agents with a realistic and rich 3d environment. *arXiv preprint arXiv:1801.02209* (2018)
38. Wu, Y., Wu, Y., Tamar, A., Russell, S., Gkioxari, G., Tian, Y.: Bayesian relational memory for semantic visual navigation. In: *Proceedings of the IEEE International Conference on Computer Vision*. pp. 2769–2779 (2019)
39. Yang, W., Wang, X., Farhadi, A., Gupta, A., Mottaghi, R.: Visual semantic navigation using scene priors. *arXiv preprint arXiv:1810.06543* (2018)
40. Yang, W., Li, X., Zhang, Z.: A regularized approach to sparse optimal policy in reinforcement learning. In: *Advances in Neural Information Processing Systems*. pp. 5938–5948 (2019)
41. Zhang, H., Goodfellow, I., Metaxas, D., Odena, A.: Self-attention generative adversarial networks. *arXiv preprint arXiv:1805.08318* (2018)
42. Zhang, J., Springenberg, J.T., Boedecker, J., Burgard, W.: Deep reinforcement learning with successor features for navigation across similar environments. In: *Proc. IROS*. pp. 2371–2378 (2017)
43. Zhu, F., Zhu, L., Yang, Y.: Sim-real joint reinforcement transfer for 3d indoor navigation. In: *Proceedings of the IEEE Conference on Computer Vision and Pattern Recognition*. pp. 11388–11397 (2019)
44. Zhu, Y., Mottaghi, R., Kolve, E., Lim, J.J., Gupta, A., Fei-Fei, L., Farhadi, A.: Target-driven visual navigation in indoor scenes using deep reinforcement learning. In: *Proc. ICRA*. pp. 3357–3364 (2017)
45. Zhu, Y., Wang, Z., Merel, J., Rusu, A., Erez, T., Cabi, S., Tunyasuvunakool, S., Kramár, J., Hadsell, R., de Freitas, N., et al.: Reinforcement and imitation learning for diverse visuomotor skills. *arXiv preprint arXiv:1802.09564* (2018)